# Comparison Study of Rotor Field-Oriented Control and Stator Field-Oriented Control in Permanent Magnet Synchronous Motors

Rashad Ghassani, Zohra Kader, Maurice Fadel, Pascal Combes, Mohammad Koteich

# Comparison Study for RFOC and SFOC in PMSMs

Rashad Ghassani
*Université de Toulouse*
*Laplace Laboratory*
Toulouse, France
rashad.ghassani@laplace.univ-tlse.fr

Zohra Kader
*Université de Toulouse*
*Laplace Laboratory*
Toulouse, France
zohra.kader@laplace.univ-tlse.fr

Maurice Fadel
*Université de Toulouse*
*Laplace Laboratory*
Toulouse, France
maurice.fadel@laplace.univ-tlse.fr

Pascal Combes
*Schneider Toshiba Inverter Europe*
Pacy-sur-Eure, France
pascal.combes@se.com

Mohammad Koteich
*Schneider Toshiba Inverter Europe*
Pacy-sur-Eure, France
mohamad.koteich@ieee.org

***Abstract*—This paper presents a comparison study between the Rotor Field-Oriented Control (RFOC) and Stator Field-Oriented Control (SFOC) for Permanent-Magnet Synchronous Motors (PMSMs). Both methods fall within the well-known Field-oriented control (FOC) category. To evaluate both methods for PMSM control, different methodologies should be provided, beginning with the control design, the Maximum Torque per Ampere (MTPA) control strategy, and the flux weakening approach. Finally, comparison between both methods based on simulation results on a 2.2kW motor model is presneted.**

***Index Terms*—Field-oriented control (FOC), Stator Flux-Oriented Control (SFOC), Rotor Flux-Oriented Control (RFOC), and Permanent Magnet Synchronous Motor (PMSM).**

## I. Introduction

Permanent Magnet Synchronous Motors (PMSMs) are widely employed across all industrial applications, with a steadily increasing market share over the last decades, especially in the automotive field [1]. Because the magnetic field is created by the magnets, the absence of rotor currents minimizes motor losses and temperature, resulting in more torque and power density, as well as a higher power factor, and thus better efficiency.

PMSM control methods can be divided into scalar and vector control (see Fig. 1). In scalar control, only the amplitude and frequency (angular speed) of voltage, current, and flux linkage space vectors are regulated based on steady-state equations. As a result, the scalar control has no effect on the position of the space vector during transients. In contrast, in vector control, not only the magnitude and frequency are adjusted, but also the instantaneous values of voltage, current, and flux space vectors [2], which allows transient operation. By controlling the space vectors in both steady-state and transient conditions, vector control has become the common control strategy used for the high-performance control of PMSMs [2].

Vector control is a generic control philosophy that may be applied differently. Direct Torque Control (DTC) [3] is a vector control approach that works in the space vector coordinates. Since it was introduced in 1985 [4], there has been continuous research and improvement in this method. In DTC the current vector control is replaced with two hysteresis controllers (bang-bang control), one for the stator flux magnitude and the other for the electromagnetic torque. Furthermore, the absence of Pulse Width Modulation (PWM) in DTC results in a variable switching frequency, which is one of the disadvantages of this method. Other types of vector control methods can be used to achieve the decoupling of PMSM equations. This gave rise to nonlinear control approaches [5], such as feedback linearization control (FLC) [6] or input-output decoupling [7].

Field-Oriented Control (FOC) introduced by Blaschke [8] is the most well-known technique that has been put in place for high-performance AC motor control. Field orientation aims to reestablish the decoupling of the flux and torque-generating components of the stator current vector, as in the case of a Direct Current (DC) motor. This control approach is based on closed-loop control of the decoupled current components. To achieve this decoupling, the machine's equations are transformed into a coordinate system that rotates in synchronism with the rotor flux vector. The FOC was presented first in the rotor coordinates (RFOC), while the stator flux orientation (SFOC) scheme was developed later on to avoid the parameter sensitivity of RFOC in the case of rotor flux estimation for induction motors [9]. Recently, the SFOC was suggested to control PMSMs mainly at high-speed applications in the flux weakening region [10]. In the literature, nonlinear controllers are equally used to improve the performances of both SFOC and RFOC approaches [11], [12], [13].

This paper presents a formal comparative study of the PMSM FOC approach, particularly RFOC and SFOC based on linear PI controllers. Indeed, RFOC based on linear PI controllers is the most widely implemented vector controller in industrial applications. Thus, to keep the comparison as fair as possible, we compare it with SFOC based on PI controllers. Section II presents the conventional model of the PMSM in the rotor- and stator-synchronous reference frames. The control design study for each method was performed in Section III. Furthermore, the Maximum Torque Per Ampere (MTPA) control strategy is studied in Section IV, while the flux weakening analysis is investigated for both methods in

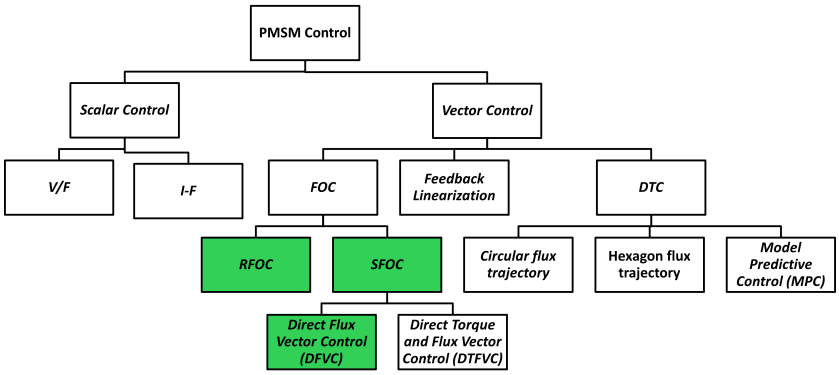


Fig. 1. Classification of PMSM control methods

Section V. Finally, the simulation results, presented in Section VI, show the performance of each method when applied to a 2.2 kW PMSM model.

## II. PMSM Model

In order to simplify the PMSM model, different assumptions are made:

- The magnetic circuit is linear (no saturation).
- Hysteresis and Foucault's currents are neglected.

### A. Motor model in rotor flux coordinates

The rotor flux-oriented (RFO) frame of PMSMs is based on the rotor flux orientation [14], which is simply the direction of the magnets' north pole (see Fig. 2). From the above assumptions, the PMSM voltage equations in the RFO frame are given as [2]:

$$v_d = R_s i_d + \frac{d\psi_d}{dt} - \omega\psi_q \tag{1}$$

$$v_q = R_s i_q + \frac{d\psi_q}{dt} + \omega\psi_d \tag{2}$$

where $v$, $i$, and $\psi$ denote the voltage, current, and flux, respectively. The stator resistance is defined by $R_s$, while $\omega$ represents the electrical angular frequency. The PMSM flux-current equation is written as:

$$\psi_d = L_d i_d + \psi_m \quad ; \quad \psi_q = L_q i_q \tag{3}$$

such that $L_d$ and $L_q$ are the $dq$-axis inductances, respectively. $\psi_m$ is the permanent magnet flux. The PMSM electromagnetic torque $T_e$ equation is:

$$T_e = \frac{3}{2} n_p(\psi_d i_q - \psi_q i_d) = \frac{3}{2} n_p(\psi_m + (L_d - L_q) i_d) i_q \tag{4}$$

where $n_p$ is the number of pole pairs of the machine. The above equation can be simplified for Surface PMSM (SPMSM), where the stator inductances are almost equal such that $L_d = L_q = L_s$.

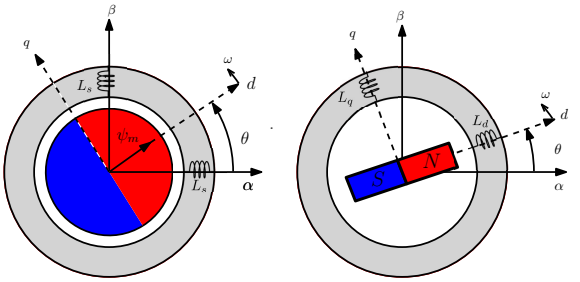


Fig. 2. SPMSM (left) and IPMSM (right) rotor flux reference frame

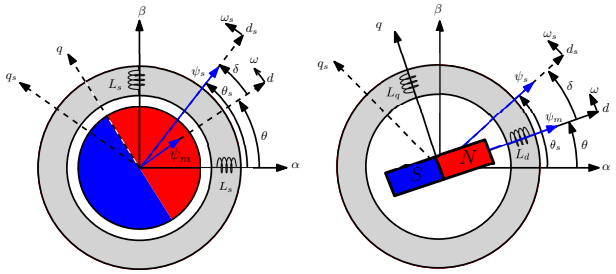


Fig. 3. Stator flux reference frame

### B. Motor model in stator flux coordinates

The stator flux-oriented (SFO) frame rotates at a synchronous speed $\omega$, such that the direct axis follows the stator magnetic flux vector $\bar{\psi}_s$ rather than the rotor magnetic flux $\bar{\psi}_m$ (see Fig. 3) [15]. The mechanical position of the rotor corresponds with the rotor flux vector. The angle $\delta$ between the stator and rotor flux vectors is defined as the load/torque angle. In the SFO frame, the stator flux is the $d_s$-axis flux:

$$\psi_{d_s} = \psi_s \quad ; \quad \psi_{q_s} = 0 \tag{5}$$

where $\psi_s$ is the amplitude of stator flux vector $\bar{\psi}_s$. Writing the voltage equations in the SFO reference frame leads to:

$$v_{d_s} = R_s i_{d_s} + \frac{d\psi_s}{dt} \tag{6}$$

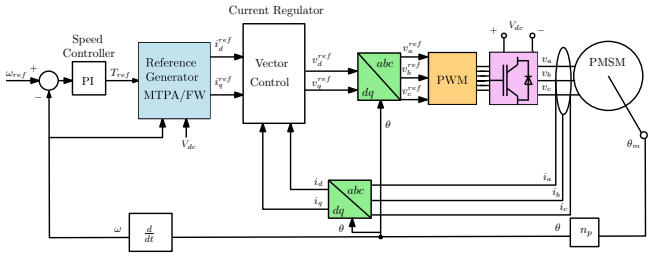


Fig. 4. RFOC complete control structure

$$v_{q_s} = R_s i_{q_s} + (\omega + \frac{d\delta}{dt})\psi_s \tag{7}$$

From (4) and (5) the torque equation in the SFO frame is then obtained as:

$$T_e = \frac{3}{2} n_p \psi_s i_{q_s} \tag{8}$$

## III. RFOC and SFOC Control Design

In this section, the controller design for both RFOC and SFOC is developed.

### A. RFOC

The RFOC of PMSMs is done in the RFO frame [16]. From (1) and (2), we obtain the $dq$ currents state space equations:

$$\begin{aligned} \frac{d}{dt}\begin{bmatrix} i_d \\ i_q \end{bmatrix} &= \begin{bmatrix} -\frac{R_s}{L_d} & \omega\frac{L_q}{L_d} \\ -\omega\frac{L_d}{L_q} & -\frac{R_s}{L_q} \end{bmatrix}\begin{bmatrix} i_d \\ i_q \end{bmatrix} \\ &+ \begin{bmatrix} \frac{1}{L_d} & 0 \\ 0 & \frac{1}{L_q} \end{bmatrix}\begin{bmatrix} v_d \\ v_q - \omega\psi_m \end{bmatrix} \end{aligned} \tag{9}$$

For controlling the currents in RFOC, a Proportional Integral (PI) current control can be implemented. There are mainly two types of PI controllers used in the literature: synchronous PI current regulator with cross-coupling decoupling and complex vector synchronous PI with active damping [17]. This study will focus on the first approach due to its similarities with the SFOC controller structure. The complete scheme for RFOC is shown in Figs. 4 and 5, such that the PI coefficients are defined as follows:

$$K_{pd} = \omega_{bc} L_d \quad ; \quad K_{pq} = \omega_{bc} L_q, \tag{10}$$

$$K_{id} = K_{iq} = \omega_{bc} R_s, \tag{11}$$

where $\omega_{bc}$ is the chosen current controller bandwidth.

### B. SFOC: Direct Flux Vector Control (DFVC)

DFVC is a control technique that utilizes the SFO frame [12], [18]. In DFVC rather than controlling the $dq$ currents, we control the torque variables which are the stator flux magnitude $\psi_s$ and the torque-producing current component $i_{qs}$. For the simplicity of control, it is important to obtain the state equation of $i_{qs}$. The vector coordinates transformation from the rotor to stator coordinates is defined as follows:

$$\begin{bmatrix} i_{d_s} \\ i_{q_s} \end{bmatrix} = \begin{bmatrix} \cos\delta & \sin\delta \\ -\sin\delta & \cos\delta \end{bmatrix}\begin{bmatrix} i_d \\ i_q \end{bmatrix} \tag{12}$$

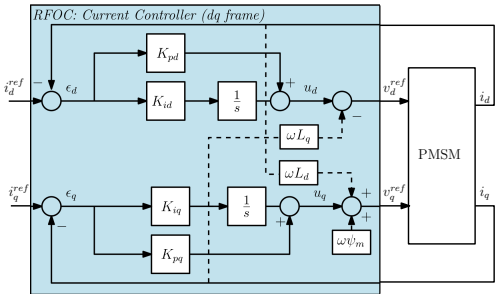


Fig. 5. PMSM PI current regulator in RFOC, shown in a rotor synchronous reference frame. Dashed lines correspond to feedforward terms

Using (12) the $q_s$-axis equation can be written as [10]:

$$L_d \frac{di_{q_s}}{dt} = -k(\delta)(v_{d_s} - R_s i_{d_s}) + b(\delta, \psi_s)(v_{q_s} - R_s i_{q_s} - \omega\psi_s) \tag{13}$$

The two factors $k(\delta)$ and $b(\delta, \psi_s)$ are defined below:

$$k(\delta) = (1 - \frac{L_d}{L_q})\frac{\sin 2\delta}{2}; \tag{14}$$

$$b(\delta, \psi_s) = -(1 - \frac{L_d}{L_q})\cos 2\delta + \frac{\psi_m \cos\delta}{\psi_s} \tag{15}$$

Note that for SPMSM, $k(\delta)$ = 0 and $b(\delta, \psi_s) = \frac{\psi_m \cos\delta}{\psi_s}$. The obtained nonlinear model of both $i_{q_s}$ and $\psi_s$ is defined as:

$$\begin{aligned} \frac{d}{dt}\begin{bmatrix} \psi_s \\ i_{q_s} \end{bmatrix} &= \begin{bmatrix} -R_s & 0 \\ \frac{k(\delta)R_s}{L_d} & -\frac{b(\delta,\psi_s)R_s}{L_d} \end{bmatrix}\begin{bmatrix} i_{d_s} \\ i_{q_s} \end{bmatrix} \\ &+ \begin{bmatrix} 1 & 0 \\ -\frac{k(\delta)}{L_d} & \frac{b(\delta,\psi_s)}{L_d} \end{bmatrix}\begin{bmatrix} v_{d_s} \\ v_{q_s} \end{bmatrix} + \begin{bmatrix} 0 \\ -\frac{b(\delta,\psi_s)}{L_d}\omega\psi_s \end{bmatrix} \end{aligned} \tag{16}$$

In contrast to RFOC, DFVC has only one current control loop. However, the current loop dynamics are nonlinear and coupled with $d_s$-axis voltage, thus derating the control performance. To control $\psi_s$ and $i_{q_s}$, both linear and nonlinear controllers [13] were proposed in the literature. In this study, we choose to compare RFOC with the SFOC scheme that uses two PI controllers. This renders the comparison fair since both approaches have the same structure. Of course, from (16), we can see that the tuning of PI controllers will depend on the nonlinear functions $b(\delta, \psi_s)$ and $k(\delta)$. Different tuning methods, such as designing the controllers by considering the best case $(b_{max})$, or taking into account the variations of $b(\delta, \psi_s)$ and $k(\delta)$ by adaptive PI controllers, can be used. In this paper, we consider that the last tuning approach is far from what is used in the traditional RFOC scheme. Moreover, adaptive controller implementation may introduce some undesirable computational complexity in industrial applications. Thus, here, the PI controllers in SFOC are tuned according to the first tuning strategy in which the tuning of PI coefficients depends on the two factors $k(\delta)$ and $b(\delta, \psi_s)$. The complete structure of DFVC is shown in Fig. 6.

*1) Flux $\psi_s$ Regulator:* The flux loop can be controlled to respond very quickly using $v_{d_s}$ according to (6) with no coupling effect from $v_{q_s}$. Aside from the discretization constraint

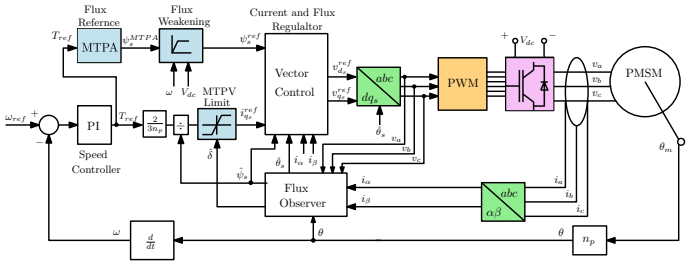


Fig. 6. SFOC complete control structure

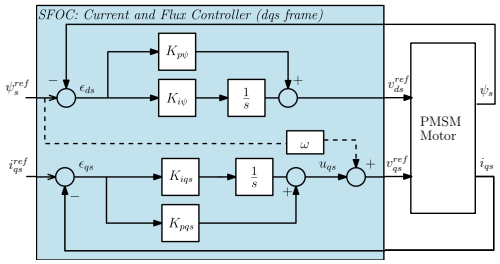


Fig. 7. PMSM PI current and flux regulator in SFOC, shown in a stator synchronous reference frame. Dashed lines correspond to feedforward terms

caused by PWM, the flux bandwidth $\omega_{bf}$ is restricted only by the dynamics of the flux observer.

*2) Current $i_{q_s}$ Regulator:* To control $i_{q_s}$ a fast PI regulator is needed to cancel the cross-coupling effect from the flux loop (16), whereas the back-EMF is compensated in a feed-forward manner. The dynamic response of $i_{q_s}$ is influenced by $b(\psi_s, \delta)$ (see (15)), which fluctuates with the motor's operating point. The vector control for both $i_{q_s}$ and $\psi_s$ is shown in Fig. 7, with PI coefficients defined as follows:

$$K_{p\psi} = \omega_{bf} \quad ; \quad K_{pq_s} = \omega_{bc}\frac{L_d}{b_{max}}, \tag{17}$$

$$K_{i\psi} = \omega_{bf}R_s \quad ; \quad K_{iq_s} = \omega_{bc}R_s, \tag{18}$$

where $b_{max}$ is the maximum value of $b(\psi_s, \delta)$.

*3) Maximum Torque Per Volt (MTPV) Limit:* The control of $i_{q_s}$ is not stable in the case $b(\psi_s, \delta) < 0$, due to positive feedback [10]. To prevent this instability, this constraint is respected by the limitation of $i_{q_s}^{ref}$ by a saturation limit.

*4) Flux Observer:* The adopted observer in our study is based on both the current and voltage models [19]. From the flux observer, we can obtain both the stator flux angle $\hat{\theta}_s$ and magnitude $\hat{\psi}_s$.

## IV. MTPA

The MTPA control strategy is an important factor in the torque generation of the Interior PMSM (IPMSMs) [20].

### A. Maximum Torque per Amper (MTPA) in RFOC

To obtain the maximum efficiency in RFOC from the motor the current references must follow the MTPA equations when possible, such that $i_{dq}^{ref}$ should be computed as follows [20]:

$$i_{d_{MTPA}} = \frac{\psi_m - \sqrt{\psi_m^2 + 8L_\Delta^2 I_s^2}}{-4L_\Delta} < 0 \tag{19}$$

where $L_\Delta = L_d - L_q < 0$

$$i_{q_{MTPA}} = sign(T_{ref})\sqrt{I_s^2 - i_{d_{MTPA}}^2} \tag{20}$$

such that the current vector magnitude $I_s$ is defined as follows:

$$I_s = \frac{2|T_{ref}|}{3n_p\psi_m} \tag{21}$$

Note that for SPMSM in RFOC, the MTPA control strategy is obtained by setting $i_{d_{MTPA}} = 0$ and $i_{q_{MTPA}} = sign(T_{ref})I_s$.

### B. MTPA in SFOC

The MTPA trajectory in SFOC is defined as the control points for achieving the maximum torque at any given flux [10]. In contrast to RFOC, SFOC controls directly the flux to produce the maximum torque. The flux reference must be set according to the MTPA curve to find the optimal flux values for a given torque.

## V. Flux Weakening (FW)

A motor can be accelerated by the maximum torque until the terminal voltage reaches its maximum value $V_{max}$, at this point, we obtain the maximum speed, defined as $\omega_{base}$ [21].

### A. FW in RFOC

In the case of RFOC, the voltage and current limited maximum torque control (VCLMT) [22] is the most employed method in the feedforward FW technique. In this method, the $i_d$ current reference is computed as follows [23]:

$$i_{d_{fw}} = \frac{-\psi_m L_d + \Delta}{L_d^2 - L_q^2} < 0 \tag{22}$$

where $\Delta$ is defined as:

$$\Delta = \sqrt{(\psi_m L_d)^2 - (L_d^2 - L_q^2)(\psi_m^2 + L_q I_s^2 - V_{max}^2/\omega^2)} \tag{23}$$

For IPMSM, $i_d$ is always negative as long as $L_d < L_q$. Where $i_{dq}^{ref}$ depends on the motor speed, which can be working either in the MTPA or FW region. If $\omega < \omega_{base}$:

$$i_d^{ref} = i_{d_{MTPA}} \quad ; \quad i_q^{ref} = i_{q_{MTPA}} \tag{24}$$

Above the base speed, the $i_d$ and $i_q$ for MTPA control cannot fulfill the voltage constraint. If $\omega > \omega_{base}$ then:

$$i_d^{ref} = i_{d_{fw}} \quad ; \quad i_q^{ref} = sign(T_{ref})\sqrt{I_s^2 - i_{d_{fw}}^2} \tag{25}$$

### B. FW in SFOC

The FW in the SFOC is simpler than in the RFOC and may be controlled directly via the flux $\psi_s$ rather than $i_d$ [24]. From (7) the flux reference is limited according to:

$$\psi_s^{ref} \leq \frac{V_{max}}{|\omega|} \tag{26}$$

And by adding the resistance drop we obtain:

$$\psi_s^{ref} \leq \frac{\sqrt{V_{max}^2 - (R_s i_{d_s})^2} - R_s i_{q_s}}{|\omega|} \tag{27}$$

## VI. Simulations and Performance Comparison

Both RFOC and SFOC were tested in simulation, using Matlab/Simulink, on the 2.2kW-motor model whose parameters are presented in Table I. To set up the simulation environment the current controller bandwidth is fixed to $\omega_{bc}$= $2\pi 100$ rad/s. While the flux loop is chosen two times faster than the current controller, so that $\omega_{bf} = 2\pi 200$ rad/s. The PI controllers of both RFOC and DFVC are tuned according to the motor parameters which are assumed to be known.

### A. Current control loops performance

To evaluate the performance of current controllers for both methods a step response (0.5 p.u) test was done at standstill on both $i_q$ and $i_{q_s}$ (Fig 9). It is obvious that RFOC has no overshoot and a faster settling time ($t_s = 5$ms) compared to SFOC $i_{q_s}$ current control ($t_s = 10$ms). This is due to the fact of the non-linearity between $v_{q_s}$ and $i_{q_s}$. To test the sensitivity of the current controllers, the $dq$-axis inductances are altered. In the case of the RFOC, the $q$-axis current loop is tested by changing $L_q$ by $\pm 30\%$, which affected the settling time with a small increase as well as a minor overshoot (see Fig. 10). As for SFOC, since $i_{q_s}$ control depends only the $d$-axis inductance (13), by decreasing $L_d$ by 30% the settling time $t_s$ increased from 10ms to 16ms (Fig. 11).

TABLE I
2.2kW PMSM Motor Nameplate

| PMSM Motor 2.2kW | |
|---|---|
| Rated Voltage | 400 [V] |
| Rated Speed | 1500 [rpm] |
| Rated Current | 4.3 [A] |
| Rated Frequency | 75 [Hz] |
| $R_s$ | 3.6 [Ω] |
| $L_d$ | 36 [mH] |
| $L_q$ | 51 [mH] |
| $\psi_m$ | 0.545 [Vs] |
| J | 0.015 [$kg.m^2$] |

### B. Torque control performance

To compare both methods, different operating points (A, B, C, D, E) are chosen in the speed-torque plane (Fig. 8). Table II shows the results for torque control performance criteria: rising time ($t_r$), settling time ($t_s$), and percentage overshoot ($PO$). It is shown that although both methods have been tuned to have the same bandwidth, RFOC has a better dynamic response than SFOC in which the rising and settling times for the torque control are faster in all the tested operating points. This difference becomes more obvious as the torque reference increases, leading to different operating points with larger torque angles. Fig. 15 shows the speed control in the FW region (point E), where it is seen that RFOC is slightly faster than SFOC. In Fig. 16 the $\psi_s$ and $i_d$ control in FW are shown. It is seen that both methods achieve almost the same tracking error in transient periods for the $i_d$ current and $\psi_s$ control. The MTPA control strategy was tested for both methods (Fig. 17), where SFOC shows a slightly better performance concerning $I_s$ as the load torque increases, thus achieving better efficiency.

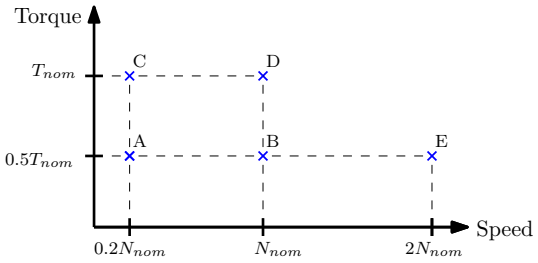


Fig. 8. Speed-torque profile operating test points

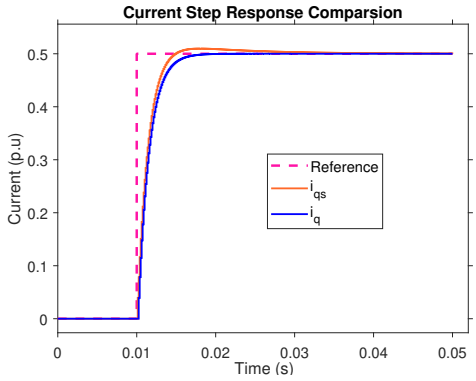


Fig. 9. Step current response comparison between RFOC and SFOC

TABLE II
Torque control performance on different operating points

| Pts | RFOC | | | SFOC | | |
|---|---|---|---|---|---|---|
| | $tr$(ms) | $ts$(ms) | $PO$(%) | $tr$(ms) | $ts$(ms) | $PO$(%) |
| A | 3.15 | 5.1 | 0 | 3.2 | 9 | 1.5 |
| B | 3.25 | 5.2 | 0 | 3.4 | 11 | 2.5 |
| C | 3.15 | 5.2 | 0.5 | 3.3 | 10 | 2.5 |
| D | 3.2 | 5.25 | 0.5 | 3.7 | 10 | 2.7 |
| E | 3.3 | 7 | 3 | 4.1 | 12 | 5 |

## VII. Conclusion

This paper presents a comparative study of RFOC and SFOC for PMSM. It is demonstrated that RFOC delivers a faster transient speed response than SFOC while keeping the control system simpler. Although the SFOC scheme is disadvantaged by parameter sensitivity and a more complex tuning to the current controller, it is seen that SFOC is advantaged by a less parameter-dependent FW control strategy . When compared with RFOC, the SFOC approach for PMSM might be viewed as a novel strategy that can be improved in terms of performance by using more advanced controllers. Finally, future studies should be focused on validating the simulations on a real PMSM hardware setup.

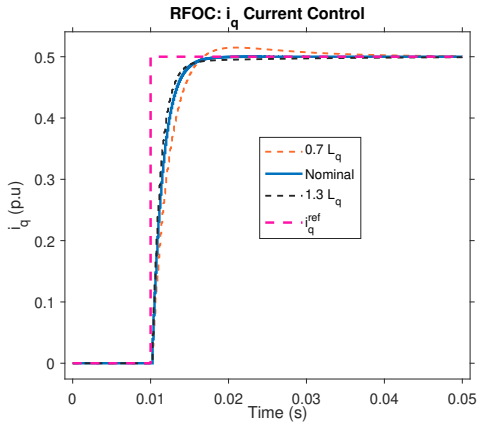


Fig. 10. $L_q$ error impact on $i_q$ control response (RFOC)

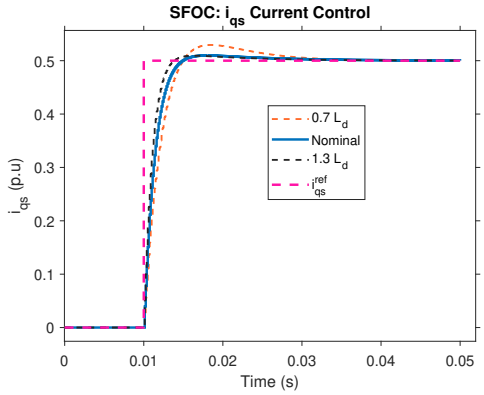


Fig. 11. $L_d$ error impact on $i_{qs}$ control response (SFOC)

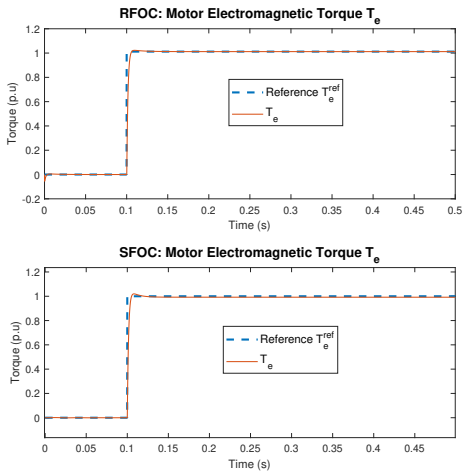


Fig. 12. Torque response for RFOC and SFOC at nominal speed (point D)

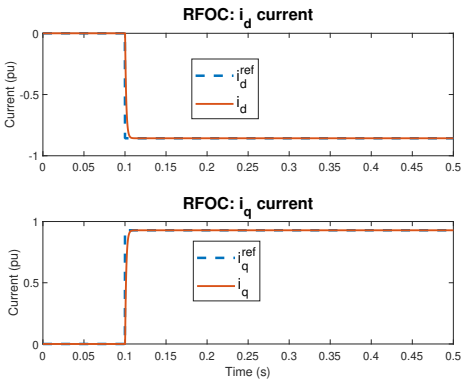


Fig. 13. RFOC current control under nominal torque reference at nominal speed (point D)

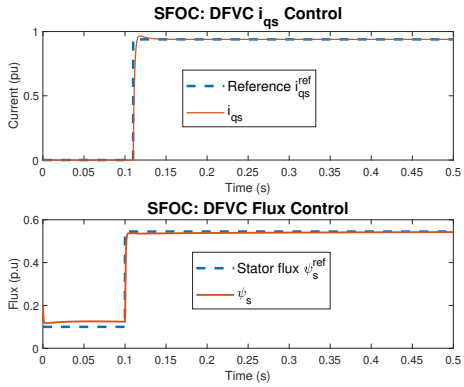


Fig. 14. SFOC flux and current control under nominal torque reference at nominal speed (point D)

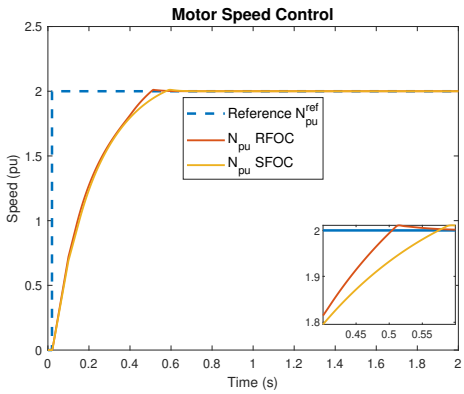


Fig. 15. Speed response in FW region (point E)

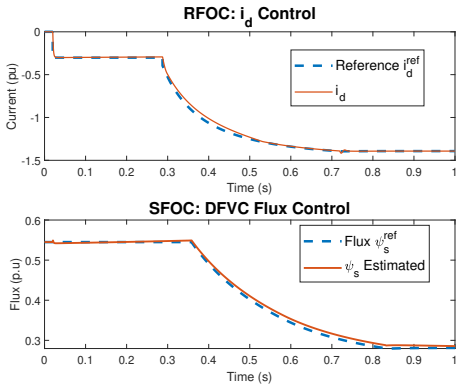


Fig. 16. $\psi_s$ and $i_d$ control in FW region (point E)

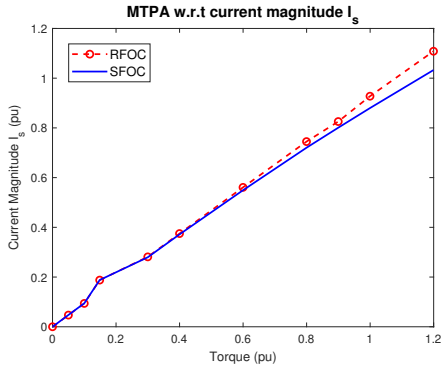


Fig. 17. MTPA in terms of current magnitude $I_s$ for both RFOC and SFOC

## REFERENCES


[1] M. Kovacik, P. Rafajdus, and S. Kocan, "Comparison of various PMSM rotor topologies for high-speed drives in automotive applications," *Transportation Research Procedia*, vol. 55, pp. 995–1002, 2021, 14th International scientific conference on sustainable, modern and safe transport, ISSN: 2352-1465. DOI: https://doi.org/10.1016/j.trpro.2021.07.070.

[2] S.-H. Kim, "Preface," in *Electric Motor Control*, S.-H. Kim, Ed., Elsevier, 2017, pp. xi–xii, ISBN: 978-0-12-812138-2. DOI: https://doi.org/10.1016/B978-0-12-812138-2.00014-3.

[3] G. Buja and M. Kazmierkowski, "Direct torque control of pwm inverter-fed ac motors - a survey," *IEEE Transactions on Industrial Electronics*, vol. 51, no. 4, pp. 744–757, 2004. DOI: 10.1109/TIE.2004.831717.

[4] P. Pillay and R. Krishnan, "Modeling, simulation, and analysis of permanent-magnet motor drives. i. the permanent-magnet synchronous motor drive," *IEEE Transactions on Industry Applications*, vol. 25, no. 2, pp. 265–273, 1989.

[5] D. Taylor, "Nonlinear control of electric machines: An overview," *IEEE Control Systems Magazine*, vol. 14, no. 6, pp. 41–51, 1994. DOI: 10.1109/37.334414.

[6] S. Xiao-Jing, "Design and simulation of pmsm feedback linearization control system," *TELKOMNIKA Indonesian Journal of Electrical Engineering*, vol. 11, Jan. 2013. DOI: 10.11591/telkomnika.v11i3.2192.

[7] M. Bodson, J. Chiasson, and R. Novotnak, "High-performance induction motor control via input-output linearization," *IEEE Control Systems Magazine*, vol. 14, no. 4, pp. 25–33, 1994. DOI: 10.1109/37.295967.

[8] F. Blaschke, "The principle of field orientation as applied to the new transvector closed-loop system for rotating-field machines," *Siemens Review*, vol. 34, no. 3, pp. 217–220, 1972.

[9] X. Xu, R. De Doncker, and D. Novotny, "A stator flux oriented induction machine drive," in *PESC '88 Record., 19th Annual IEEE Power Electronics Specialists Conference*, 1988, 870–876 vol.2. DOI: 10.1109/PESC.1988.18219.

[10] G. Pellegrino, E. Armando, and P. Guglielmi, "Direct flux field-oriented control of ipm drives with variable dc link in the field-weakening region," *IEEE Transactions on industry Applications*, vol. 45, pp. 1619 –1627, Nov. 2009. DOI: 10.1109/TIA.2009.2027167.

[11] J. Solsona, M. Valla, and C. Muravchik, "Nonlinear control of a permanent magnet synchronous motor with disturbance torque estimation," *IEEE Transactions on Energy Conversion*, vol. 15, no. 2, pp. 163–168, 2000. DOI: 10.1109/60.866994.

[12] G. Pellegrino, R. I. Bojoi, and P. Guglielmi, "Unified direct-flux vector control for ac motor drives," *IEEE Transactions on Industry Applications*, vol. 47, no. 5, pp. 2093–2102, 2011. DOI: 10.1109/TIA.2011.2161532.

[13] H. A. A. Awan, M. Hinkkanen, R. Bojoi, and G. Pellegrino, "Stator-flux-oriented control of synchronous motors: A systematic design procedure," *IEEE Transactions on Industry Applications*, vol. 55, no. 5, pp. 4811–4820, 2019. DOI: 10.1109/TIA.2019.2927316.

[14] F. Briz and M. Hinkkanen, "Design, implementation and performance of synchronous current regulators for ac drives," *Chinese Journal of Electrical Engineering*, vol. 4, no. 3, pp. 53–65, 2018.

[15] H. Hofmann, S. Sanders, and A. EL-Antably, "Stator-flux-oriented vector control of synchronous reluctance machines with maximized efficiency," *IEEE Transactions on Industrial Electronics*, vol. 51, no. 5, pp. 1066–1072, 2004. DOI: 10.1109/TIE.2004.834968.

[16] F. Briz, M. Degner, and R. Lorenz, "Analysis and design of current regulators using complex vectors," *IEEE Transactions on Industry Applications*, vol. 36, no. 3, pp. 817–825, 2000. DOI: 10.1109/28.845057.

[17] D. F. Laborda, J. M. Guerrero, M. O. Zapico, D. Fernández, D. D. Reigosa, and F. Briz, "Online pi current controller tuning based on machine high-frequency parameters," in *2021 IEEE Energy Conversion Congress and Exposition (ECCE)*, 2021, pp. 5029–5035. DOI: 10.1109/ECCE47101.2021.9595336.

[18] G. Pellegrino, E. Armando, and P. Guglielmi, "Direct-flux vector control of ipm motor drives in the maximum torque per voltage speed range," *IEEE Transactions on Industrial Electronics*, vol. 59, no. 10, pp. 3780–3788, 2012. DOI: 10.1109/TIE.2011.2178212.

[19] P. Guglielmi, M. Pastorelli, G. Pellegrino, and A. Vagati, "Position-sensorless control of permanent-magnet-assisted synchronous reluctance motor," *Industry Applications, IEEE Transactions on*, vol. 40, pp. 615 –622, Apr. 2004. DOI: 10.1109/TIA.2004.824438.

[20] S. Liu, W. Huang, X. Lin, Y. Zhao, W. Jiang, and J. Yang, "Maximum torque per ampere control based on active flux concept for dtc of ipmsms," in *2018 IEEE Energy Conversion Congress and Exposition (ECCE)*, 2018, pp. 6558–6562.

[21] L. Sepulchre, M. Fadel, M. Pietrzak-David, and G. Porte, "Mtpv flux-weakening strategy for pmsm high-speed drive," *IEEE Transactions on Industry Applications*, vol. 54, no. 6, pp. 6081–6089, 2018. DOI: 10.1109/TIA.2018.2856841.

[22] L. Sepulchre, "Pour l'optimisation de la commande des machines synchrones à aimants permanents en régime de haute vitesse pour véhicule électrique," 2017. [Online]. Available: https://oatao.univ-toulouse.fr/17839/.

[23] M. Fadel, L. Sepulchre, and M. Pietrzak-David, "Deep flux-weakening strategy with mtpv for high-speed ipmsm for vehicle application," *IFAC-PapersOnLine*, vol. 51, no. 28, pp. 616–621, 2018, 10th IFAC Symposium on Control of Power and Energy Systems CPES 2018, ISSN: 2405-8963. DOI: https://doi.org/10.1016/j.ifacol.2018.11.772.

[24] R. Bojoi, P. Guglielmi, and G. Pellegrino, "Sensorless stator field-oriented control for low cost induction motor drives with wide field weakening range," in *2008 IEEE Industry Applications Society Annual Meeting*, 2008, pp. 1–7. DOI: 10.1109/08IAS.2008.18.